Investigating the urban air quality effects of cool walls and cool roofs in Southern California

Jiachen Zhang[1], Yun Li[1], Wei Tao[2], Junfeng Liu[3], Ronnen Levinson[4], Arash Mohegh[1], George Ban-Weiss[1,*]

[1] Department of Civil and Environmental Engineering, University of Southern California, Los Angeles, CA, USA

[2] Multiphase Chemistry Department, Max-Planck-Institute for Chemistry, Hahn-Meitner-Weg 1, Mainz, Germany

[3] Laboratory for Earth Surface Processes, College of Urban and Environmental Sciences, Peking University, Beijing, China

[4] Heat Island Group, Lawrence Berkeley National Laboratory, Berkeley, CA, USA

*Correspondence to George Ban-Weiss, banweiss@usc.edu, 213-740-9124

Abstract

Solar reflective cool roofs and walls can be used to mitigate the urban heat island effect. While many past studies have investigated the climate impacts of adopting cool surfaces, few studies have investigated their effects on air pollution, especially on particulate matter (PM). This research for the first time investigates the influence of widespread deployment of cool walls on urban air pollutant concentrations, and systematically compares cool wall to cool roof effects. Simulations using a coupled meteorology-chemistry model (WRF-Chem) for a representative summertime period show that cool walls and roofs can reduce urban air temperatures, wind

speeds, and planetary boundary heights in the Los Angeles Basin. Consequently, increasing wall (roof) albedo by 0.80, an upper bound scenario, leads to maximum daily 8-hour average ozone concentration reductions of 0.35 (0.83) ppbv in Los Angeles County. However, cool walls (roofs) increase daily average $PM_{2.5}$ concentrations by 0.62 (0.85) μg m^{-3}. We investigate the competing processes driving changes in concentrations of speciated $PM_{2.5}$. Increases in primary PM (elemental carbon and primary organic aerosols) concentrations can be attributed to reductions in ventilation of the Los Angeles Basin. Increases in concentrations of semi-volatile species (e.g., nitrate) are mainly driven by increases in gas-to-particle conversion due to reduced atmospheric temperatures.

1 Introduction

Urbanization is occurring at a fast pace around the world; global urban land area in 2030 is projected to be up to triple that in 2000[1]. Compared to rural areas with natural land cover, urban areas contain more impervious surfaces that are made of solar absorptive and thermally massive materials, such as asphalt concrete. Urban areas also contain less vegetation and thus reduced evaporative cooling and shade cover. These differences in urban and natural land cover contribute to the urban heat island (UHI) effect (i.e., cities being hotter than their surrounding rural areas)[2], which can, in turn, affect air pollutant concentrations. The air quality effects of urban land expansion have been studied in previous research[3–7], although only a few studies clearly explained the mechanisms driving these effects[8–11]. Tao et al.[8] suggested that with pollutant emissions held constant, urbanization in eastern China would increase ozone concentrations from the surface to 4

km. However, it would also enhance turbulent mixing and vertical advection, therefore reducing the concentrations of primary pollutants below 500 m.

While many studies have explored the air quality impacts of the UHI effect, fewer studies have investigated how strategies that mitigate the UHI effect would influence urban air quality[12–15]. For example, adopting solar reflective cool surfaces (roofs, walls, and pavements) increases city albedo and the solar radiation reflected by cities, therefore reducing urban surface temperatures and near-surface air temperatures[16–22]. However, adopting cool surfaces might change air quality in unexpected ways. For primary pollutants (i.e., pollutants directly emitted to the atmosphere) such as elemental carbon (EC), nitric oxide (NO), and carbon monoxide (CO), lower surface temperatures in cities may suppress convection and therefore reduce atmospheric mixing heights and vertical dispersion of pollutants, leading to increases in pollutant concentrations near the ground[23]. Changes in horizontal temperature distributions can also influence wind speed and direction, affecting the horizontal transport and distribution of pollutants. For secondary pollutants (i.e., pollutants formed in the atmosphere from primary pollutants), in addition to the previously mentioned changes in transport and dispersion of pollutants and their precursors, pollutant concentrations can also be influenced by temperature dependent chemical reactions, phase-partitioning, and emissions. Tropospheric ozone is primarily formed via reactions between nitrogen oxides (NO_x) and volatile organic compounds (VOCs). Reductions in dispersion could increase both VOC and NO_x concentrations, though impacts on ozone could be counterintuitive due to non-linearities in ozone chemistry. Lowering air temperature decreases biogenic VOC emissions from vegetation, potentially reducing ozone concentrations in urban areas where VOC availability limits ozone formation[24]. Air temperature reduction also slows reactions that produce ozone. Therefore, ozone concentrations are expected to decrease with lower temperatures[25].

Secondary particulate matter includes sulfate, nitrate, ammonium, and secondary organic aerosols (SOA). While temperature-dependent reactions that form secondary particulate matter should be slower due to reduced temperatures, gas-particle partitioning for semi-volatile species (ammonium nitrate and semi-volatile SOA) favors the particle phase[26,27]. The competing physical and chemical processes lead to uncertainties in changes to air pollution concentrations induced by heat island mitigation strategies.

The complexity of the aforementioned processes requires the use of sophisticated models that resolve atmospheric physics and chemistry to predict how cool surface adoption would influence city-level air quality. Using photochemical models, Taha et al.[13,28] estimated that increasing city surface albedo would effectively reduce ozone concentrations in Southern California and Central California. Epstein et al.[23] predicted that 8-hour daily maximum ozone concentrations would decrease if cool roofs do not reflect more solar ultraviolet (UV) than do dark roofs; if solar UV reflection is increased, ozone concentrations could rise.

Despite previous literature on the influence of cool roofs on ozone concentrations, there is only one study that has investigated the influence of cool roofs on particulate matter[23]. They found that increasing roof albedo would increase the annual mean concentrations of $PM_{2.5}$, because reduced ventilation would suppress dispersion of pollutants. However, they did not investigate (1) the various physicochemical processes driving cool roof impacts on $PM_{2.5}$ concentrations or (2) the varying responses of different PM species (e.g., nitrate, sulfate, and organics) to cool roof adoption.

Cool walls are less studied than cool roofs. Zhang et al.[29], for the first time, estimated the influence of cool walls on urban climate, and systematically compared the effects of cool walls to cool roofs. They found that adopting cool walls in Los Angeles would lead to daily average canyon air

temperature reductions of up to 0.40 K, which is slightly lower than that induced by adopting cool roofs (0.43 K). However, the influence of cool walls on air quality has never been studied.

To address the aforementioned science knowledge gaps and inform policymaking on heat mitigation strategies, we seek to (1) quantify and systematically compare the air quality effects of adopting cool walls and roofs, and (2) investigate the physicochemical processes leading to changes in particulate matter concentrations.

2 Method

2.1 Model description

We use the Weather Research and Forecasting model coupled with Chemistry Version 3.7 (WRF-Chem V3.7), a state-of-the-science climate and air quality model, to estimate the impacts of employing cool walls and roofs on air quality[30]. WRF-Chem has been widely used to study air pollution in Southern California[11,31,32]. Table S2 summarizes our model configuration. The following schemes are chosen for WRF physics: the Rapid Radiative Transfer Model (RRTM) for long-wave radiation[33], the Goddard shortwave radiation scheme[34], the Lin et al. scheme[35] for cloud microphysics, the Grell 3D ensemble cumulus cloud scheme[36], and the Yonsei University scheme for the planetary boundary layer[37].

Impervious fraction (Figure S3b) and land use classification in urban grid cells (Figure S3c) are obtained from the National Land Cover Database (NLCD, 2006)[38,39]. The Noah land surface model[40] simulates land-atmosphere interactions in non-urban grid cells and for the pervious portion of urban grid cells. The single-layer urban canopy model resolves urban physics and

simulates land-atmosphere interactions for the impervious portion of urban grid cells[41]. Urban grid cells are classified as low-intensity residential ("Developed, Open Spaces" and "Developed, Low Intensity" in NLCD), high-intensity residential ("Developed, Medium Intensity" in NLCD), and commercial/industrial ("Developed, High Intensity" in NLCD). Urban morphology (i.e., roof width, canyon floor width, and building height) is determined for each urban land use type based on real-world building and street datasets for Los Angeles County, following Zhang et al[29]; the datasets include National Urban Database and Access Portal (NUDAPT)[42], the Los Angeles Region Imagery Acquisition Consortium (LARIAC)[42], and LA County Street and Address File[43]. Since the default WRF-Chem is not compatible with the NLCD land use classification system, we modify the model code to allow for use of NLCD urban land use types, following Fallmann et al.[44]. We also implement satellite-based green vegetation fraction into the model following Vahmani and Ban-Weiss[21].

Gas phase chemistry is simulated using the Regional Atmospheric Chemistry Mechanism (RACM)[45] scheme, further updated by National Oceanic and Atmospheric Administration (NOAA) Earth System Research Laboratory (ESRL)[32]. The RACM-ESRL scheme covers organic and inorganic chemistry simulating 23 photolysis and 221 other chemical reactions[46]. The Modal Aerosol Dynamics Model for Europe (MADE) simulates aerosol chemistry[47]. The volatility basis set (VBS) is used for simulating secondary organic aerosols[48].

We evaluate modeled ozone and $PM_{2.5}$ concentrations against observations (Figures S1 and S2, Table S1) from the Environmental Protection Agency's Air Quality System in Section S1 of the Supporting Information. Although our model underestimates ozone and $PM_{2.5}$ concentrations at higher concentrations, the bias in baseline concentrations does not necessarily lead to bias in estimated changes induced by adopting cool surfaces.

2.2 Simulation domains

We simulate three nested domains (d1, d2, and d3, as shown in Figure S3a) with 30 layers in the vertical at horizontal resolutions of 18 km, 6 km, and 2 km, respectively. The three domains each cover the Southwestern United States (d1); Central and Southern California (d2); and Southern California, including Los Angeles and San Diego (d3). Each outer domain provides boundary conditions for the adjacent inner domain. In this paper we report results for the innermost domain.

2.3 Emission inventories

WRF-Chem requires gridded emissions inputs for each simulation. We use state-of-the-science emission inventories from the South Coast Air Quality Management District (SCAQMD) and California Air Resources Board (CARB) for the year 2012 (i.e., the most up-to-date inventories as of writing this paper). For the outer two domains (d1 and d2), hourly emissions for the entire year at 4-km resolution are provided by CARB for California[49]. Emissions outside California, but within the simulation domain, are from National Emissions Inventory (NEI) by the Environmental Protection Agency for the year 2011[50]. For the innermost domain (d3), we use hourly emissions for the entire year at 4-km resolution provided by SCAQMD[51] . These emissions represent all anthropogenic sources including motor vehicles; point sources such as refineries; and off-road sources, such as construction. Emission inventories are regridded to match the grid for the modeled domains and chemical speciation for RACM-ESRL and MADE/VBS mechanisms used in this study. The Model of Emissions of Gases and Aerosols from Nature (MEGAN) is used to generate temperature-dependent biogenic organic emissions[52]. Note that anthropogenic emissions are not

sensitive to ambient temperatures in our study. Though some anthropogenic emissions may be temperature dependent (e.g., evaporative emissions of VOCs from gasoline powered vehicles), this effect is not simulated in this study, as anthropogenic emissions are obtained directly from input datasets.

2.4 Simulation design

To investigate the air quality effects of cool walls and roofs in Southern California, we simulate three scenarios: CONTROL, where wall, roof, and pavement albedos are each set to 0.10; COOL_WALL, where wall albedo is increased to 0.90; and COOL_ROOF, where roof albedo is increased to 0.90. These cool surface albedos are intentionally chosen to quantify the upper bound effects of adopting cool surfaces (i.e., increasing surface albedo by 0.80). Note that cool surface albedos of actual cool walls and roofs are usually lower than 0.90. For example, the albedo of a bright-white cool roof may decrease to 0.60–0.70 from an initial albedo of 0.80–0.90 after several years of soiling and weathering[53,54]. In order to test the linearity of changes in air pollutant concentrations to albedo increases, we add two additional scenarios where wall albedo and roof albedo are each increased by 0.40.

Simulations are performed for 28 June 2012 to 11 July 2012, with the first five days discarded as model "spin-up" to reduce the possible influence of inaccuracies in input initial conditions on our analysis. We analyze the results from 00:00 local standard time (LST) on July 3 to 00:00 LST on July 12. Section S3 in the Supporting Information demonstrates that the meteorology during our analysis period is representative of summertime meteorology in Southern California. Thus, our results are representative of changes induced by adopting cool surfaces under typical summertime

conditions in Southern California. The paired Student's t-test (n = 9 analyzed days) is used to assess whether the changes in cool surface scenarios relative to CONTROL are statistically distinguishable from zero.

2.5 Method of attributing the changes in PM to ventilation versus other factors

Carbon monoxide (CO) is considered a chemically inert pollutant at urban scale, with concentrations controlled by meteorological conditions. Therefore, past studies have used CO as a tracer for transport and dispersion of pollutants[9,56]. Similarly, in our study, we use the increase in CO concentration relative to CONTROL to quantify the increase in $PM_{2.5}$ that is attributable to ventilation ($\Delta C_{PM(\text{vent})}$), as

$$\Delta C_{PM(\text{vent})} = \frac{\Delta C_{\text{CO}}}{C_{\text{CO}}} \times C_{PM} \quad (1)$$

where ΔC_{CO} is the change in CO mixing ratio (ppbv) relative to CONTROL, C_{CO} is the mixing ratio (ppbv) of CO for CONTROL, C_{PM} is the concentration (μg m^{-3}) of a PM species (i.e., total $PM_{2.5}$, sulfate, nitrate, elemental carbon, primary organic aerosol, anthropogenic secondary organic aerosols, or biogenic secondary organic aerosols) for CONTROL, and all variables are spatial averages over urban areas in Los Angeles County.

The change in concentration of a $PM_{2.5}$ species that is not attributable to ventilation $\Delta C_{PM(\text{no vent})}$ (μg m^{-3}) is then calculated as

$$\Delta C_{PM(\text{no vent})} = \Delta C_{PM} - \frac{\Delta C_{\text{CO}}}{C_{\text{CO}}} \times C_{PM} \quad (2)$$

In this way, we attribute increases in $PM_{2.5}$ species to reductions in ventilation and changes in all other processes. Note that while sea salt aerosols contribute to total $PM_{2.5}$ concentrations, we omit this species from the discussion because they are naturally produced and are not a public health concern. Reductions in ventilation may also contribute to less vertical mixing and consequent reductions in dry deposition of pollutants.

2.6 Caveats

In this study, we assume that adopting cool surfaces would not change reflectance in the UV spectrum (280–400 nm). However, based on spectral reflectance measurements, UV reflectance could increase from adopting cool roofs[23]. Increases in UV reflectance could enhance ozone production and atmospheric oxidation capacity, which influences the formation of other secondary pollutants. Therefore, changes in ozone are a result of competing effects among (a) ozone increases induced by enhanced UV reflection, (b) ozone decreases induced by decreased temperatures, and (c) ozone changes induced by reduced ventilation, which could affect the dispersion of ozone and its precursors.

The influence of adopting cool surfaces is likely to vary by city due to differences in baseline climate and land cover (e.g., vegetation distributions, building distributions, urban canyon morphology). Also note that results might be different if simulated using another model or using different parameterizations. For example, the single layer urban canopy model does not explicitly resolve individual buildings.

Note that the urban morphology is derived using gross wall area (including windows) instead of net wall area (excluding windows). In Los Angeles County, citywide ratio of net wall area to gross wall area is 83%.[29] In reality, windows may not be changed to cool colors. Therefore, a portion of

217 walls may not be able to be made solar reflective and our study may overestimate the influence of
218 adopting cool walls.
219

220 3 Results and discussion

221 By comparing changes in air pollutant concentrations for increasing albedo by 0.80 versus 0.40
222 relative to CONTROL, we find that the changes in air pollutant concentrations are approximately
223 linear to surface albedo change (Section S4 in the Supporting Information). Therefore, the results
224 reported for albedo increase of 0.80 can be interpolated to other albedo changes. For simplicity,
225 we report only results for COOL_WALL and COOL_ROOF in the main body.

226 3.1 Meteorological conditions

227 Figure 1 shows spatial distributions of near-surface air temperatures in the afternoon and evening.
228 (Diurnal cycles of near-surface air temperatures are shown in Figure S4.) For the CONTROL
229 scenario (Figure 1a), temperatures in inland areas are hotter than coastal areas, as expected.
230 Temperature reductions induced by adopting cool surfaces are higher in inland areas than in coastal
231 areas (Figure 1b,c). This is due to an accumulation effect in air temperature reduction as the sea
232 breeze advects air from the coast to inland.

233 Although total wall area in Los Angeles County is larger than roof area by a factor of 1.7, daily
234 average solar irradiance (W m^{-2}) on walls is 38% of that on roofs[29]. In addition, 50-59% of the
235 solar radiation reflected by cool walls is absorbed by opposing walls or pavements, while all the
236 radiation reflected by cool roofs escapes the urban canopy in the model[29]. Therefore, daily average
237 temperature reductions induced by cool roofs (0.45 K) are larger than cool walls (0.24 K) over

urban areas in Los Angeles County, as shown in Table 1. Cool roofs are simulated to induce larger temperature reductions than cool walls at both 14:00 LST (daytime) and 20:00 LST (nighttime).

Note that past studies investigating how air temperatures influence atmospheric chemistry often report 2-meter air temperatures ("T2")[8,45]. However, 2-meter air temperature is a diagnostic variable that is not used in model calculations of atmospheric chemistry. The chemistry model actually uses the four-dimensional (x, y, z, t) atmospheric temperature. Therefore, we present temperatures in the lowest atmospheric layer as "near-surface air temperature" rather than "T2."

Figures S5 and S6 show diurnal cycles and spatial maps of 10-meter horizontal wind speeds, and Figure S7 shows horizontal wind vectors. For the CONTROL scenario, winds are southwesterly from coast to inland and wind speed is higher during daytime than nighttime. As shown in Table 1, spatially averaged wind speed in urban areas is 4.2 m s^{-1} and 2.3 m s^{-1} at 14:00 LST and 20:00 LST, respectively. Simulations predict that adopting cool walls (roofs) decreases onshore wind speeds by 0.06 (0.21) m s^{-1} at 14:00 LST and 0.08 (0.09) m s^{-1} at 20:00 LST. This can be explained by the reduced temperature difference between urban land and ocean, which is a driver for the sea breeze.

Figure S8 show the diurnal cycle of planetary boundary layer (PBL) height. PBL height reaches its maximum at 12:00 LST. Adopting cool walls reduces PBL height by 3-7% at most times of day. Adopting cool roofs reduces PBL height by about 5% at night and about 10% during the day. The reduction in PBL height can be attributed to decreases in surface temperatures and consequent reductions in convection. Decreases in wind speeds and PBL height tend to reduce ventilation for pollutants. The influence of changes in ventilation on particulate matter is discussed in Section 3.5.1.

3.2 Spatial distribution of ozone concentrations

Figure 2 shows the spatial distribution of daily maximum 8-hour average (MDA8) ozone concentrations. MDA8 ozone is regulated by the National Ambient Air Quality Standards of the Environmental Protection Agency. For the CONTROL scenario, the ozone concentration over urban areas is lower than rural areas because (a) southwesterly winds transport ozone and its precursors from the coast to the inland areas, creating an accumulation effect as this secondary pollutant is generated in the atmosphere; and (b) nitric oxide emissions in urban areas can titrate ozone. Adopting cool walls can decrease the spatially averaged MDA8 ozone concentration by 0.35 ppbv in the urban areas of Los Angeles County (Table 1). These decreases in ozone concentrations are likely due to reductions in temperature-dependent ozone formation. Adopting cool roofs can lead to a greater reduction in MDA8 ozone concentration (0.83 ppbv) than cool walls. This is likely because the near-surface air temperature reductions induced by cool roofs are larger than that induced by cool walls during daytime (Figure S4) and thus the decreases in reaction rates for ozone production are larger for COOL_ROOF than COOL_WALL relative to CONTROL. As mentioned in Section 2.5, we assume that the UV reflectance of cool surfaces is the same as dark surfaces. Similarly, Epstein et al[23] report reductions in ozone concentrations in most Southern California regions due to adopting cool roofs when UV reflectance is assumed to be held constant. (Note that they also find that ozone concentrations could increase if the difference in UV reflectance between cool and dark roofs follows an upper bound scenario.)

3.3 Spatial distribution of $PM_{2.5}$ species

Figure 3 shows the spatial distribution of daily average $PM_{2.5}$ species concentrations and changes due to adopting cool surfaces. $PM_{2.5}$ concentrations reported here represent dry particle mass. Spatial distributions of $PM_{2.5}$ species concentrations in the CONTROL scenario are mainly attributable to spatial patterns in emissions and meteorology. For example, when the sea breeze advects air from the coast to inland, EC, a primary pollutant, accumulates, leading to higher concentrations in locations further east. For spatial distributions of sulfate concentrations, there are higher concentrations near the ports of Los Angeles and Long Beach that are likely due to hot spots in SO_2 (the precursor of secondary sulfate) and primary sulfate emissions from ships and power plants (Figure S9). Meanwhile, southwesterly winds then transport these emissions to downtown Los Angeles, making concentrations downtown greater than those further east. The spatial variability of anthropogenic and biogenic SOA is relatively small compared to other species.

The concentrations of total $PM_{2.5}$ and each individual species increase due to cool surface adoption (Figure 3). The increase in each $PM_{2.5}$ species induced by adopting cool roofs is larger than that induced by cool walls, though their spatial patterns are similar. Spatial distributions of increases in total $PM_{2.5}$ and individual species (except nitrate) are consistent with the spatial patterns of absolute concentrations in the CONTROL scenario. In other words, the regions with the highest baseline concentrations show the largest changes in $PM_{2.5}$ due to meteorological shifts from cool surface adoption. The exception is for nitrate, which shows larger increases in urban residential areas northeast of downtown where baseline concentrations are low, rather than downtown where baseline concentrations are the highest in CONTROL. This is likely due to the greater temperature reductions in regions northeast of downtown Los Angeles relative to downtown, especially at night (Figure 1b,c). The processes leading to nitrate increases will be discussed in Section 3.5. The

increase in SOA is relatively smaller than other species, which will also be explained in Section 3.5.

3.4 Diurnal cycles of $PM_{2.5}$ species concentrations

Figure 4 shows the diurnal cycles of spatially averaged $PM_{2.5}$ species concentrations and their changes in the urban areas of Los Angeles County. For the CONTROL scenario, $PM_{2.5}$, nitrate, ammonium, sulfate, EC, and primary organic aerosol (POA) concentrations reach their maximum between 08:00 and 09:00 LST and their minimum at 16:00 LST, while biogenic and anthropogenic SOA reach their maximum near 14:00 LST and their minimum at night. The diurnal cycles of $PM_{2.5}$ concentrations can be attributed to the diurnal variation of (1) emissions (Figure S10); (2) PBL height (Figure S8a), which peaks at 12:00 LST; (3) wind speed (Figure S5), which peaks at 14:00 LST; and (4) photochemical reaction rates for secondary species that depend on UV radiation and temperature (Figure S4a).

Raising roof or wall albedo leads to increases in concentrations of total $PM_{2.5}$ and most individual species (except for biogenic SOA) throughout the day (Figure 4). Increases in nitrate concentrations are the largest among all $PM_{2.5}$ species, followed by increases in POA, sulfate, and ammonium, while the increases in concentrations of other $PM_{2.5}$ species are relatively small. The changes in speciated $PM_{2.5}$ concentrations due to adopting cool walls or roofs vary by time of day, and the mechanisms contributing to the changes will be discussed in Section 3.5. For all $PM_{2.5}$ species except biogenic SOA, increases in $PM_{2.5}$ concentrations induced by adopting cool roofs are larger than those induced by adopting cool walls during most daytime hours (07:00-19:00 LST). On daily average, cool roof adoption contributes to greater increases in particulate matter than cool wall adoption (Table 1) for total $PM_{2.5}$ and each species. Daily average increases in total $PM_{2.5}$ concentrations are simulated to be 0.62 (0.85) $\mu g\ m^{-3}$ upon increasing wall (roof) albedo by 0.80

in July in Los Angeles County. Compared to the national annual and 24-hour $PM_{2.5}$ standard of 12 μg m^{-3} and 35 μg m^{-3}, respectively, increases in $PM_{2.5}$ concentrations reported here have the potential for increasing exceedance days of federal air quality standards. The grid cell containing Mira Loma (i.e., the most polluted $PM_{2.5}$ monitoring station in Southern California) is simulated to have $PM_{2.5}$ increases of 0.84 (1.05) μg m^{-3} due to adopting cool walls (roofs) in summer. Epstein et al. (2018) estimate that annual average $PM_{2.5}$ concentrations at Mira Loma would increase by 0.19 μg m^{-3} due to adopting cool roofs, which they compute would result in an increase of 2/3 exceedance day for the 24-hr federal $PM_{2.5}$ standard. (The number of exceedance days is not an integer because they report 3x3 cell moving averages.) Thus, even though these changes may look small, they have the potential to increase the annual number of days exceeding air quality standards and are therefore important for regulatory agencies in controlling $PM_{2.5}$ pollution.

3.5 Mechanisms that lead to changes in $PM_{2.5}$ concentrations

As mentioned in the introduction, adopting cool surfaces can influence $PM_{2.5}$ concentrations mainly via (1) reducing ventilation, (2) slowing temperature dependent reactions and emissions, and (3) increasing the likelihood that semi-volatile species will partition to particle phase. In the following sections we report on the relative importance of these pathways.

3.5.1 Ventilation

For primary pollutants such as elemental carbon (EC), mass concentrations depend highly on ventilation and are insensitive to atmospheric chemistry in the model. (Note that strictly speaking, hydrophilic species can coat EC and increase its hygroscopicity, enabling the in-cloud wet scavenging of EC[56]. This so-called "aging process" depends on temperature-dependent atmospheric photochemical reactions that form hydrophilic species, such as sulfate. However, the

aging of EC should not be a very important process during summer when there is little precipitation in the Los Angeles Basin.) Decreases in ventilation (Section 3.1) impede the dilution and transport of pollutants in source regions and may also reduce dry deposition, leading to increases in near-surface pollutant concentrations. This ventilation effect is driven by vertical and horizontal mixing of pollutants in the planetary boundary layer, which can be investigated using PBL height and surface wind speeds, respectively. Figure 5 shows that fractional increase in EC is positively correlated with the fractional reductions in PBL height and 10-meter wind speed. Fractional reduction in PBL height can explain 42% of the variability in the fractional increase in EC concentrations for both COOL_WALL – CONTROL and COOL_ROOF – CONTROL. Fractional reduction in horizontal wind speed explains 17% (79%) of the variability in fractional increase of EC concentrations due to adopting cool walls (roofs).

3.5.2 Quantifying the relative importance of ventilation versus other factors for driving changes in PM

Following the method described in Section 2.5, we quantify increases in $PM_{2.5}$ species that can be attributed to reductions in ventilation and changes in other processes. As indicated in Figure 4, after removing the effects of ventilation, the change in spatially averaged EC and POA is close to zero. Therefore, increases in primary pollutant (EC and POA) concentrations are attributable to suppressed ventilation. A large fraction of the increase in sulfate from cool surface adoption can be attributed to suppressed ventilation. Other driving processes can affect sulfate concentrations: (a) reductions in temperature-dependent reaction rates would decrease sulfate production; and (b) changes in cloud cover can also influence in-cloud SO_2 oxidation, which occurs faster than gas-phase oxidation of SO_2 if clouds are present. When the ventilation effect is excluded, sulfate concentrations slightly increase from 04:00 to 14:00 LST but decrease at most other hours, due to

adopting cool surfaces. Nevertheless, ventilation is the dominant process leading to sulfate increases, contributing to 76 % (91%) of the daily average increase for COOL_WALL – CONTROL (COOL_ROOF – CONTROL).

On the other hand, the ventilation effect accounts for a small portion of the increase in semi-volatile species such as nitrate and ammonium (in the form of ammonium nitrate). Concentrations of these particulate species rise drastically even when the ventilation effect is excluded. This is because the reaction between gas-phase ammonia and nitric acid that forms particulate nitrate is reversible, and the equilibrium constant for the reaction is highly temperature dependent. Temperature reductions would cause gas to particle conversion and increase the concentrations of ammonium nitrate[26]. Note that the amount of nitrate at equilibrium has a non-linear relationship with temperature. Thus, the relationship between increase in nitrate concentration due to gas-to-particle conversion (Figure 4) and temperature reduction is not linear; the increase in nitrate depends not only on the magnitude of temperature reduction but also the baseline temperature. In contrast to shifting equilibrium of the reaction between nitric acid and ammonia, which would increase nitrate, cool surfaces adoption may also reduce photochemistry and impede the formation of nitric acid precursors (i.e., OH and NO_2) during the day, leading to a reduction in nitrate. Increased gas-to-particle conversion and suppressed ventilation outweigh reductions in photochemistry, leading to overall increases in nitrate concentrations (Figure 4).

For secondary organic aerosols (SOA), reductions in ventilation should lead to increases in SOA, while temperature decreases would be expected to cause (a) increases in gas-to-particle conversion for semi-volatile species, which would lead to SOA increases, and (b) reduced rates of temperature-dependent reactions, which would lead to SOA decreases. Biogenic SOA may also be influenced by reductions in temperature dependent VOC emissions (e.g., isoprene) from

vegetation (Figure S11). As shown in Figure 4, both anthropogenic and biogenic SOA increase when including the influence of changes in ventilation, but decrease when ventilation changes are excluded. Daily average SOA concentrations increase by 0.018 (0.046) μg m^{-3} for COOL_WALL (COOL_ROOF) relative to CONTROL. After removing the ventilation effect, daily average SOA concentrations decrease by 0.057 (0.071) μg m^{-3} for COOL_WALL (COOL_ROOF) relative to CONTROL. This means that SOA reductions induced by slowed temperature dependent reactions and biogenic emissions outweigh the expected increases in semi-volatile SOA species due to phase partitioning. On the other hand, increases in SOA due to suppressed ventilation and increased gas-to-particle conversion outweigh decreases in SOA due to reduced reaction and emission rates. These competing effects lead to an overall increase in SOA concentrations, although fractional increases are small relative to other species.

In this paper, we discuss the climate and air quality implications of cool roofs and cool walls, which have been used in cities to reduce temperatures and thus combat global warming and urban heat islands. Our results show that reductions in urban surface temperatures lead to both co-benefits of reduced ozone concentrations and penalties of increased $PM_{2.5}$ concentrations, potentially changing the exceedance days of federal air quality standard in the Los Angeles Basin. We suggest further studies to assess the air quality effects of other heat strategies and the effects in other cities. For policy makers, it is important to assess the effects of environmental solutions from a systematic perspective, i.e., looking at heat mitigation impacts not just from a climate perspective but also from an air quality perspective.

Acknowledgements

This research was supported by the California Energy Commission under contract EPC-14-010, and the National Science Foundation under grants CBET-1512429 and 1752522. This work was also supported by the Assistant Secretary for Energy Efficiency and Renewable Energy, Building Technologies Office of the U.S. Department of Energy under Contract No. DE-AC02-05CH11231. Computation for the work described in this paper was supported by the University of Southern California's Center for High-Performance Computing (https://hpcc.usc.edu/). We thank Scott Epstein and Sang-Mi Lee at South Coast Air Quality Management District for providing us emission datasets. We also thank Pouya Vahmani, Haley Gilbert, Pablo Rosado, Hugo Destaillats, and Xiaochen Tang at Lawrence Berkeley National Laboratory, Dan Li at Boston University, Ravan Ahmadov and Stu McKeen at National Oceanic and Atmospheric Administration, Joachim Fallmann at Johannes Gutenberg University Mainz, Gert-Jan Steeneveld at Wageningen University, and Jan Kleissl at University of California, San Diego for their helpful suggestions.

Supporting Information

Model evaluation, description of the simulated period, and further detail on results. This material is available free of charge via the Internet at http://pubs.acs.org.

References

(1) Seto, K. C.; Guneralp, B.; Hutyra, L. R. Global Forecasts of Urban Expansion to 2030 and Direct

Impacts on Biodiversity and Carbon Pools. *Proc. Natl. Acad. Sci.* **2012**, *109* (40), 16083–16088.

(2) Oke, T. R. City Size and the Urban Heat Island. *Atmos. Environ. Pergamon Pres* **1973**, *7*, 769–779.

(3) Civerolo, K.; Hogrefe, C.; Lynn, B.; Rosenthal, J.; Ku, J. Y.; Solecki, W.; Cox, J.; Small, C.; Rosenzweig, C.; Goldberg, R.; Knowlton, K.; Kinney, P. Estimating the Effects of Increased Urbanization on Surface Meteorology and Ozone Concentrations in the New York City Metropolitan Region. *Atmos. Environ.* **2007**, *41* (9), 1803–1818.

(4) Li, J.; Georgescu, M.; Hyde, P.; Mahalov, A.; Moustaoui, M. Achieving Accurate Simulations of Urban Impacts on Ozone at High Resolution. *Environ. Res. Lett.* **2014**, *9* (11), 114019.

(5) Wang, X. M.; Lin, W. S.; Yang, L. M.; Deng, R. R.; Lin, H. A Numerical Study of Influences of Urban Land-Use Change on Ozone Distribution over the Pearl River Delta Region, China. *Tellus B Chem. Phys. Meteorol.* **2007**, *59* (3), 633–641.

(6) Stone, B. Urban Sprawl and Air Quality in Large US Cities. *J. Environ. Manage.* **2008**, *86* (4), 688–698.

(7) Zhong, S.; Qian, Y.; Sarangi, C.; Zhao, C.; Leung, R.; Wang, H. Urbanization Effect on Winter Haze in the Yangtze River Delta Region of China. *Geophys. Res. Lett.* **2018**, *45* (13), 6710–6718.

(8) Tao, W.; Liu, J.; Ban-Weiss, G. A.; Hauglustaine, D. A.; Zhang, L.; Zhang, Q.; Cheng, Y.; Yu, Y.; Tao, S. Effects of Urban Land Expansion on the Regional Meteorology and Air Quality of Eastern China. *Atmos. Chem. Phys.* **2015**, *15* (15), 8597–8614.

(9) Tao, W.; Liu, J.; Ban-Weiss, G. A.; Zhang, L.; Zhang, J.; Yi, K.; Tao, S. Potential Impacts of Urban Land Expansion on Asian Airborne Pollutant Outflows. *J. Geophys. Res.* **2017**, *122* (14), 7646–7663.

(10) Sarrat, C.; Lemonsu, A.; Masson, V.; Guedalia, D. Impact of Urban Heat Island on Regional

458 Atmospheric Pollution. *Atmos. Environ.* **2006**, *40* (10), 1743–1758.

459 (11) Li, Y.; Zhang, J.; Sailor, D. J.; Ban-weiss, G. A. Effects of Urbanization on Regional Meteorology
460 and Air Quality in Southern California. *Atmos. Chem. Phys.* **2019**, *19* (7), 4439–4457.

461 (12) Rosenfeld, A. H.; Akbari, H.; Romm, J. J.; Pomerantz, M. Cool Communities: Strategies for Heat
462 Island Mitigation and Smog Reduction. *Energy Build.* **1998**, *28* (1), 51–62.

463 (13) Taha, H. Meso-Urban Meteorological and Photochemical Modeling of Heat Island Mitigation.
464 *Atmos. Environ.* **2008**, *42* (38), 8795–8809.

465 (14) Taha, H.; Chang, S.; Akbari, H. Meteorological and Air Quality Impacts of Heat Island Mitigation
466 Measures in Three U.S. Cities. *Energy* **2000**, No. April.

467 (15) Taha, H. Meteorological, Air-Quality, and Emission-Equivalence Impacts of Urban Heat Island
468 Control in California. *Sustain. Cities Soc.* **2015**, *19*, 207–221.

469 (16) Zhang, J.; Zhang, K.; Liu, J.; Ban-Weiss, G. Revisiting the Climate Impacts of Cool Roofs around
470 the Globe Using an Earth System Model. *Environ. Res. Lett.* **2016**, *11* (8), 084014.

471 (17) Mohegh, A.; Rosado, P.; Jin, L.; Millstein, D.; Levinson, R.; Ban-Weiss, G. Modeling the Climate
472 Impacts of Deploying Solar Reflective Cool Pavements in California Cities. *J. Geophys. Res.*
473 **2017**, *122* (13), 6798–6817.

474 (18) Taha, H.; Konopacki, S.; Gabersek, S. Impacts of Large-Scale Surface Modifications on
475 Meteorological Conditions and Energy Use: A 10-Region Modeling Study. *Theor. Appl. Climatol.*
476 **1999**, *62* (3–4), 175–185.

477 (19) Georgescu, M.; Morefield, P. E.; Bierwagen, B. G.; Weaver, C. P. Urban Adaptation Can Roll
478 Back Warming of Emerging Megapolitan Regions. *Proc. Natl. Acad. Sci.* **2014**, *111* (8), 2909–
479 2914.

(20) Li, D.; Bou-Zeid, E.; Oppenheimer, M. The Effectiveness of Cool and Green Roofs as Urban Heat Island Mitigation Strategies. *Environ. Res. Lett.* **2014**, *9* (5), 055002.

(21) Vahmani, P.; Ban-Weiss, G. Climatic Consequences of Adopting Drought-Tolerant Vegetation over Los Angeles as a Response to California Drought. *Geophys. Res. Lett.* **2016**, *43* (15), 8240–8249.

(22) Mohegh, A.; Levinson, R.; Taha, H.; Gilbert, H.; Zhang, J.; Li, Y.; Tang, T.; Ban-Weiss, G. Observational Evidence of Neighborhood Scale Reductions in Air Temperature Associated with Increases in Roof Albedo. *Climate* **2018**, *6* (4), 98.

(23) Epstein, S. A.; Lee, S.-M.; Katzenstein, A. S.; Carreras-Sospedra, M.; Zhang, X.; Farina, S. C.; Vahmani, P.; Fine, P. M.; Ban-Weiss, G. Air-Quality Implications of Widespread Adoption of Cool Roofs on Ozone and Particulate Matter in Southern California. *Proc. Natl. Acad. Sci.* **2017**, 201703560.

(24) Nowak, D. J.; McHale, P. J.; Ibarra, M.; Crane, D.; Stevens, J. C.; Luley, C. J. Modeling the Effects of Urban Vegetation on Air Pollution. *Air Pollut. Model. its Appl. XII* **1998**, 399–407.

(25) Taha, H. Modeling the Impacts of Large-Scale Albedo Changes on Ozone Air Quality in the South Coast Air Basin. *Atmos. Environ.* **1997**, *31* (11), 1667–1676.

(26) Moya, M.; Ansari, A. S.; Pandis, S. N. Partitioning of Nitrate and Ammonium between the Gas and Particulate Phases during the 1997 IMADA-AVER Study in Mexico City. *Atmos. Environ.* **2001**, *35* (10), 1791–1804.

(27) Pun, B. K.; Griffin, R. J.; Seigneur, C.; Seinfeld, J. H. Secondary Organic Aerosol 2. Thermodynamic Model for Gas/Particle Partitioning of Molecular Constituents. *J. Geophys. Res. Atmos.* **2002**, *107* (D17), AAC-4.

(28) Taha, H. Urban Surface Modification as a Potential Ozone Air-Quality Improvement Strategy in

California: A Mesoscale Modelling Study. *Boundary-Layer Meteorol.* **2008**, *127* (2), 219–239.

(29) Zhang, J.; Mohegh, A.; Li, Y.; Levinson, R.; Ban-Weiss, G. Systematic Comparison of the Influence of Cool Wall versus Cool Roof Adoption on Urban Climate in the Los Angeles Basin. *Environ. Sci. Technol.* **2018**, *52* (19), 11188–11197.

(30) Grell, G. A.; Peckham, S. E.; Schmitz, R.; McKeen, S. A.; Frost, G.; Skamarock, W. C.; Eder, B. Fully Coupled "Online" Chemistry within the WRF Model. *Atmos. Environ.* **2005**, *39* (37), 6957–6975.

(31) Chen, D.; Li, Q.; Stutz, J.; Mao, Y.; Zhang, L.; Pikelnaya, O.; Tsai, J. Y.; Haman, C.; Lefer, B.; Rappenglück, B.; Alvarez, S. L.; Neuman, J. A.; Flynn, J.; Roberts, J. M.; Nowak, J. B.; de Gouw, J.; Holloway, J.; Wagner, N. L.; Veres, P.; Brown, S. S.; Ryerson, T. B.; Warneke, C.; Pollack, I. B. WRF-Chem Simulation of NOx and O3 in the L.A. Basin during CalNex-2010. *Atmos. Environ.* **2013**, *81*, 421–432.

(32) Kim, S. W.; Heckel, A.; Frost, G. J.; Richter, A.; Gleason, J.; Burrows, J. P.; McKeen, S.; Hsie, E. Y.; Granier, C.; Trainer, M. NO_2 Columns in the Western United States Observed from Space and Simulated by a Regional Chemistry Model and Their Implications for NO_x Emissions. *J. Geophys. Res. Atmos.* **2009**, *114* (11), 1–29.

(33) Mlawer, E. J.; Taubman, S. J.; Brown, P. D.; Iacono, M. J.; Clough, S. A. Radiative Transfer for Inhomogeneous Atmospheres: RRTM, a Validated Correlated-k Model for the Longwave. *J. Geophys. Res. Atmos.* **1997**, *102* (D14), 16663–16682.

(34) Chou, M.; Suarez, M. J. A Solar Radiation Parameterization for Atmospheric Studies. Technical Report Series on Global Modeling and Data Assimilation 1999.

(35) Lin, Y.-L.; Farley, R. D.; Orville, H. D.; Lin, Y.-L.; Farley, R. D.; Orville, H. D. Bulk Parameterization of the Snow Field in a Cloud Model. *J. Clim. Appl. Meteorol.* **1983**, *22* (6),

1065–1092.

(36) Grell, G. A.; Dévényi, D. A Generalized Approach to Parameterizing Convection Combining Ensemble and Data Assimilation Techniques. *Geophys. Res. Lett.* **2002**, *29* (14), 38-1-38–4.

(37) Hong, S.-Y.; Noh, Y.; Dudhia, J. A New Vertical Diffusion Package with an Explicit Treatment of Entrainment Processes. *Mon. Weather Rev.* **2006**, *134* (9), 2318–2341.

(38) Wickham, J. D.; Stehman, S. V.; Gass, L.; Dewitz, J.; Fry, J. A.; Wade, T. G. Accuracy Assessment of NLCD 2006 Land Cover and Impervious Surface. *Remote Sens. Environ.* **2013**, *130*, 294–304.

(39) Fry, J. A.; Xian, G.; Jin, S.; Dewitz, J. A.; Homer, C. G.; Yang, L.; Barnes, C. A.; Herold, N. D.; Wickham, J. D. Completion of the 2006 National Land Cover Database for the Conterminous United States. *Photogramm. Eng. Remote Sensing* **2011**, *77*, 858–566.

(40) Chen, F.; Dudhia, J.; Chen, F.; Dudhia, J. Coupling an Advanced Land Surface–Hydrology Model with the Penn State–NCAR MM5 Modeling System. Part I: Model Implementation and Sensitivity. *Mon. Weather Rev.* **2001**, *129* (4), 569–585.

(41) Kusaka, H.; Kondo, H.; Kikegawa, Y.; Kimura, F. A Simple Single-Layer Urban Canopy Model for Atmospheric Models: Comparison with Multi-Layer and Slab Models. *Boundary-Layer Meteorol.* **2001**, *101* (3), 329–358.

(42) Ching, J.; Brown, M.; Burian, S.; Chen, F.; Cionco, R.; Hanna, A.; Hultgren, T.; McPherson, T.; Sailor, D.; Taha, H.; Williams, D. National Urban Database and Access Portal Tool. *Bull. Am. Meteorol. Soc.* **2009**, *90* (8), 1157–1168.

(43) LARIAC. Countywide Building Outlines https://egis3.lacounty.gov/dataportal/lariac/ (accessed Jul 11, 2017).

(44) CAMS. LA County Street & Address File https://egis3.lacounty.gov/dataportal/2014/06/16/2011-

549 la-county-street-centerline-street-address-file (accessed Aug 3, 2017).

550 (45) Fallmann, J.; Forkel, R.; Emeis, S. Secondary Effects of Urban Heat Island Mitigation Measures
551 on Air Quality. *Atmos. Environ.* **2016**, *125*, 199–211.

552 (46) Stockwell, W. R.; Kirchner, F.; Kuhn, M.; Seefeld, S. A New Mechanism for Regional
553 Atmospheric Chemistry Modeling. *J. Geophys. Res. Atmos.* **1997**, *102* (D22), 25847–25879.

554 (47) Ahmadov, R.; McKeen, S.; Trainer, M.; Banta, R.; Brewer, A.; Brown, S.; Edwards, P. M.; De
555 Gouw, J. A.; Frost, G. J.; Gilman, J.; Helmig, D.; Johnson, B.; Karion, A.; Koss, A.; Langford, A.;
556 Lerner, B.; Olson, J.; Oltmans, S.; Peischl, J.; Pétron, G.; Pichugina, Y.; Roberts, J. M.; Ryerson,
557 T.; Schnell, R.; Senff, C.; Sweeney, C.; Thompson, C.; Veres, P. R.; Warneke, C.; Wild, R.;
558 Williams, E. J.; Yuan, B.; Zamora, R. Understanding High Wintertime Ozone Pollution Events in
559 an Oil- and Natural Gas-Producing Region of the Western US. *Atmos. Chem. Phys.* **2015**, *15* (1),
560 411–429.

561 (48) Ackermann, I. J.; Hass, H.; Memmesheimer, M.; Ebel, A.; Binkowski, F. S.; Shankar, U. Modal
562 Aerosol Dynamics Model for Europe Development and First Applications. *Atmos. Environ.* **1998**,
563 *32* (17), 2981–2999.

564 (49) Ahmadov, R.; McKeen, S. A.; Robinson, A. L.; Bahreini, R.; Middlebrook, A. M.; de Gouw, J. A.;
565 Meagher, J.; Hsie, E.-Y.; Edgerton, E.; Shaw, S.; Trainer, M. A Volatility Basis Set Model for
566 Summertime Secondary Organic Aerosols over the Eastern United States in 2006. *J. Geophys.*
567 *Res. Atmos.* **2012**, *117* (D6), n/a-n/a.

568 (50) California Air Resources Board. ARB's Emission Inventory Activities
569 https://www.arb.ca.gov/ei/ei.htm (accessed Jun 18, 2017).

570 (51) USEPA. Profile of the 2011 National Air Emissions Inventory (U.S. EPA 2011 NEI Version 1.0).
571 **2014**, No. April, 23.

(52) South Coast Air Quality Management District. Final 2016 Air Quality Management Plan, Appendix III: Base and Future Year Emission Inventory http://www.aqmd.gov/docs/default-source/clean-air-plans/air-quality-management-plans/2016-air-quality-management-plan/final-2016-aqmp/appendix-iii.pdf (accessed Jun 18, 2018).

(53) Guenther, A.; Karl, T.; Harley, P.; Wiedinmyer, C.; Palmer, P. I.; Geron, C. Estimates of Global Terrestrial Isoprene Emissions Using MEGAN (Model of Emissions of Gases and Aerosols from Nature). *Atmos. Chem. Phys.* **2006**, *6* (11), 3181–3210.

(54) Sleiman, M.; Ban-Weiss, G.; Gilbert, H. E.; François, D.; Berdahl, P.; Kirchstetter, T. W.; Destaillats, H.; Levinson, R. Soiling of Building Envelope Surfaces and Its Effect on Solar Reflectance - Part I: Analysis of Roofing Product Databases. *Sol. Energy Mater. Sol. Cells* **2011**, *95* (12), 3385–3399.

(55) Berdahl, P.; Akbari, H.; Levinson, R.; Miller, W. A. Weathering of Roofing Materials - An Overview. *Constr. Build. Mater.* **2008**, *22* (4), 423–433.

(56) Zhang, Q.; Quan, J.; Tie, X.; Li, X.; Liu, Q.; Gao, Y.; Zhao, D. Effects of Meteorology and Secondary Particle Formation on Visibility during Heavy Haze Events in Beijing, China. *Sci. Total Environ.* **2015**, *502*, 578–584.

(57) Zhang, J.; Liu, J.; Tao, S.; Ban-Weiss, G. A. Long-Range Transport of Black Carbon to the Pacific Ocean and Its Dependence on Aging Timescale. *Atmos. Chem. Phys.* **2015**, *15* (20), 11521–11535.

592

593

594 Table 1. Spatially averaged meteorological variables and pollutant concentrations for the CONTROL
595 scenario, and the change relative to CONTROL for COOL_WALL and COOL_ROOF. Values represent
596 spatial averages in Los Angeles County (shown in Figure S3b) for urban grid cells from 00:00 LST on July 3
597 to 00:00 LST on July 12.

	CONTROL	COOL_WALL minus CONTROL	COOL_ROOF minus CONTROL
Daily average near-surface air temperature [a] (K)	292.85	-0.24	-0.45
10-meter wind speed at 14:00 LST (m s^{-1})	4.15	-0.06	-0.21
10-meter wind speed at 20:00 LST (m s^{-1})	2.28	-0.08	-0.09
Daily maximum 8-hour average ozone concentration (ppbv)	38.47	-0.35	-0.83
Daily average $PM_{2.5}$ concentration (μg m^{-3})	12.25	0.62	0.85
Daily average nitrate concentration [b] (μg m^{-3})	0.89	0.11	0.18
Daily average ammonium concentration [b] (μg m^{-3})	0.98	0.07	0.10
Daily average sulfate concentration [b] (μg m^{-3})	1.91	0.11	0.13
Daily average EC concentration [b] (μg m^{-3})	0.87	0.05	0.06
Daily average anthropogenic SOA concentration [b] (μg m^{-3})	1.22	0.01	0.04
Daily average biogenic SOA concentration [b] (μg m^{-3})	0.51	0.01	0.01
Daily average POA concentration [b] (μg m^{-3})	1.90	0.12	0.14

598 [a] Near-surface air temperature refers to the temperature in the lowest atmospheric layer.

599 [b] Mass concentrations for particles with diameter less than 2.5 μm (i.e., nuclei and accumulation mode)
600 are included for each species.

601

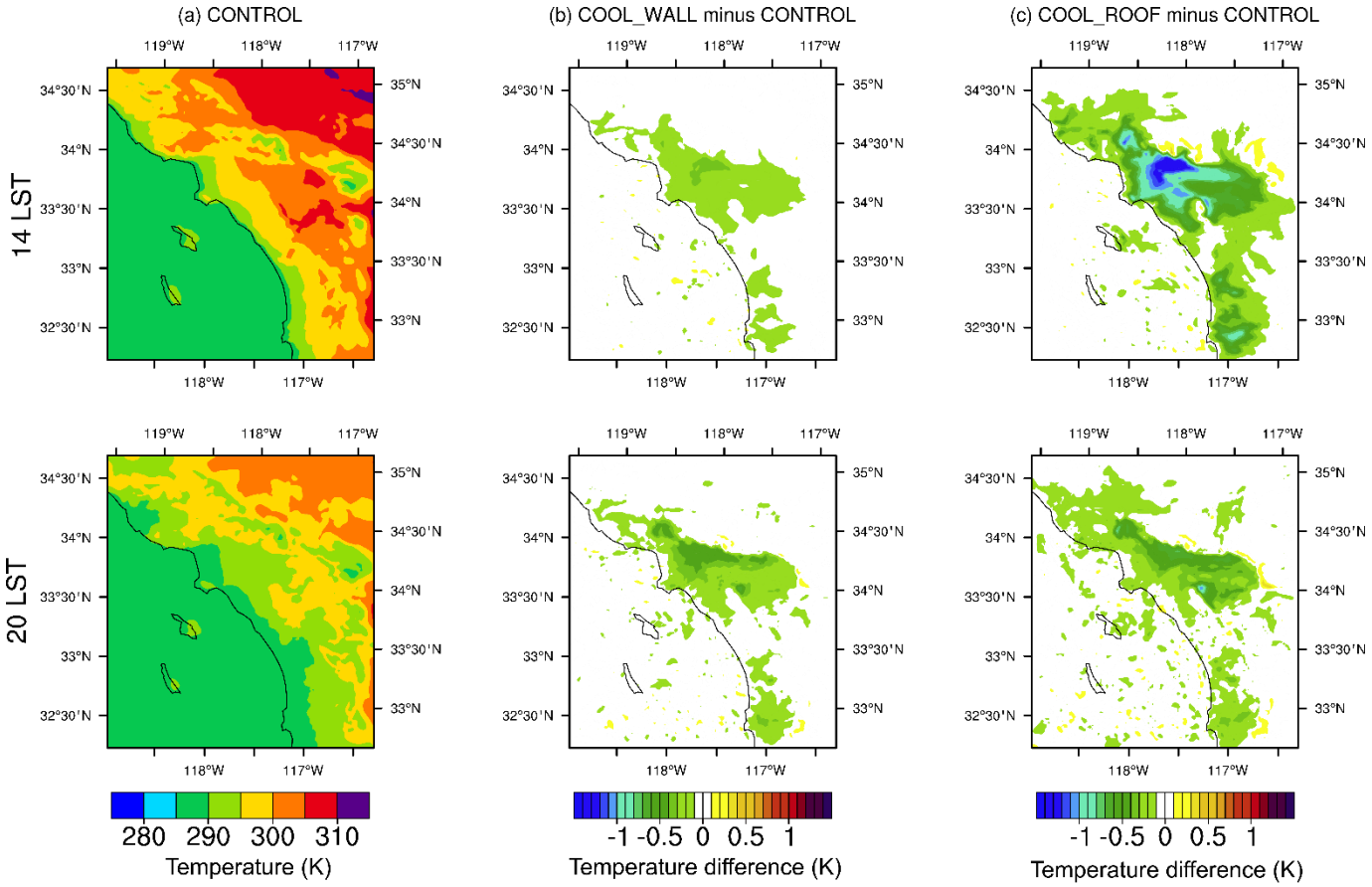

Figure 1. Spatially resolved near-surface air temperatures (K) at 14:00 LST and 20:00 LST for (a) the CONTROL scenario, and the difference relative to CONTROL for (b) COOL_WALL and (c) COOL_ROOF. Values are temporally averaged over the period of 00:00 LST on July 3 to 00:00 LST on July 12.

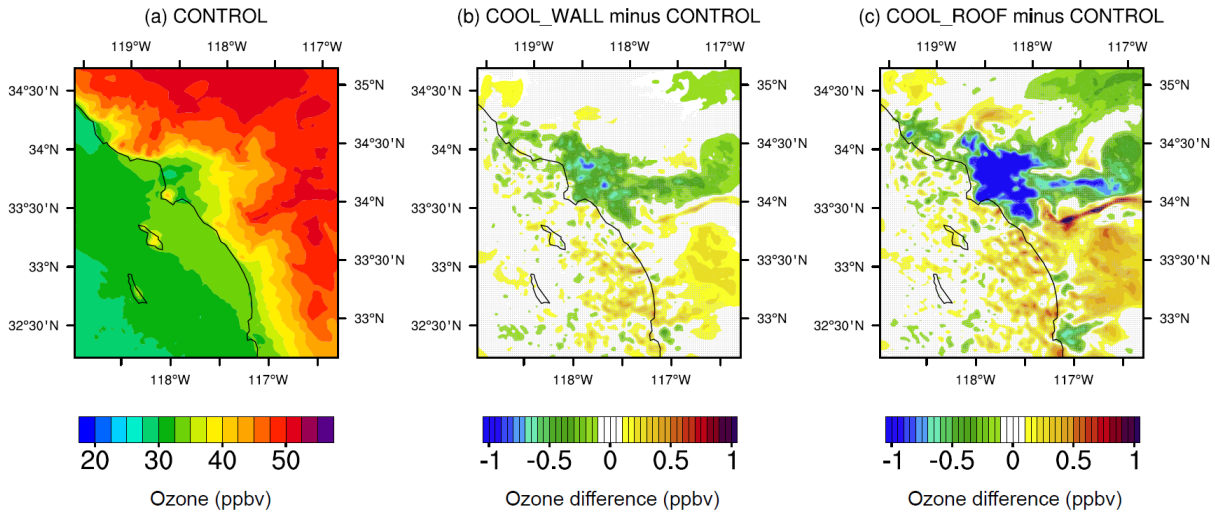

Figure 2. Spatially resolved daily maximum 8-hour average (MDA8) ozone concentrations (ppbv) for (a) the CONTROL scenario, and changes relative to CONTROL for (b) COOL_WALL and (c) COOL_ROOF. Changes that are not statistically distinguishable from zero (see section 2.4 for details on statistical analysis) in (b) and (c) are dotted. Values are temporally averaged over the period of 00:00 LST on July 3 to 00:00 LST on July 12.

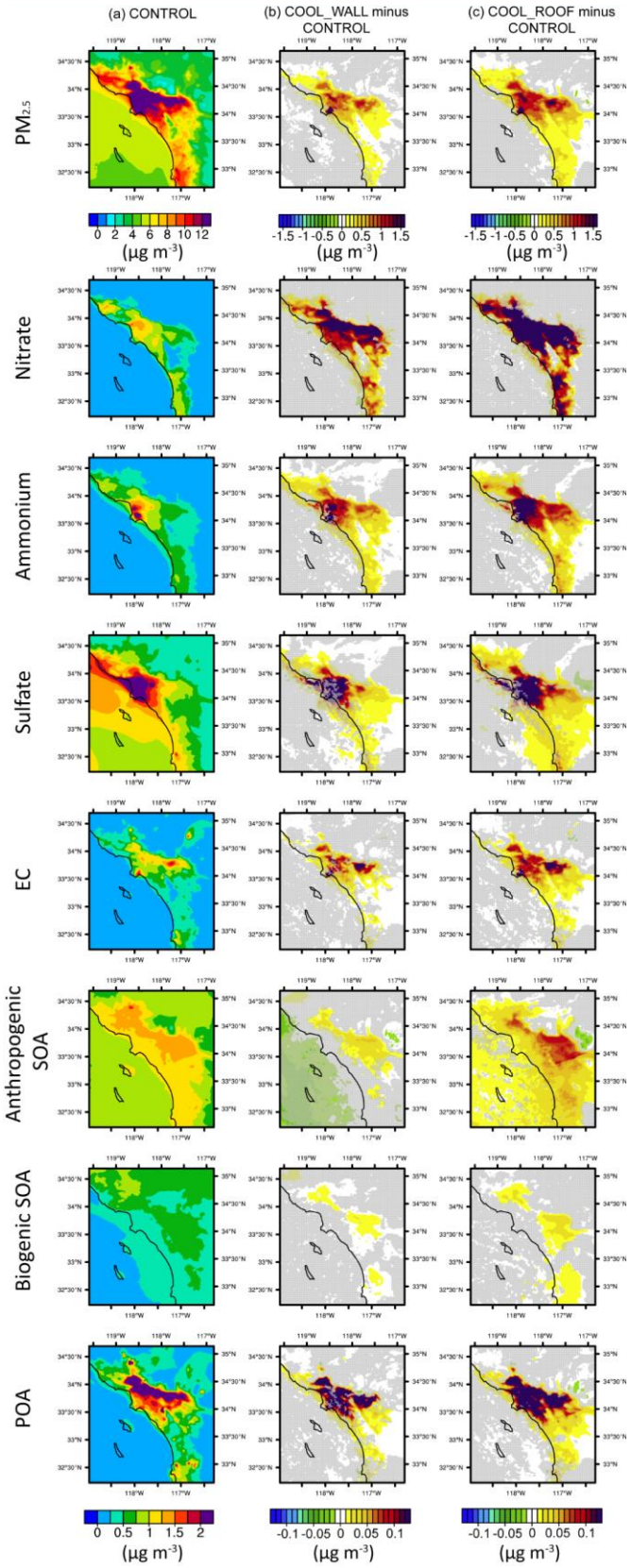
(a) CONTROL
(b) COOL_WALL minus CONTROL
(c) COOL_ROOF minus CONTROL
PM2.5
Nitrate
Ammonium
Sulfate
EC
Anthropogenic SOA
Biogenic SOA
POA
0 2 4 6 8 10 12
(μg m-3)
-1.5 -1 -0.5 0 0.5 1 1.5
(μg m-3)
-1.5 -1 -0.5 0 0.5 1 1.5
(μg m-3)
0 0.5 1 1.5 2
(μg m-3)
-0.1 -0.05 0 0.05 0.1
(μg m-3)
-0.1 -0.05 0 0.05 0.1
(μg m-3)

618

Figure 3. Daily average $PM_{2.5}$ concentrations (μg m^{-3}) by species for CONTROL (left column), as well as the differences for COOL_WALL – CONTROL (middle column) and COOL_ROOF – CONTROL (right column). Differences that are not statistically distinguishable from zero (see Section 2.4 for details on statistical analysis) are shaded in gray (middle and right columns of panels). Values are temporally averaged over the period of 00:00 LST on July 3 to 00:00 LST on July 12.

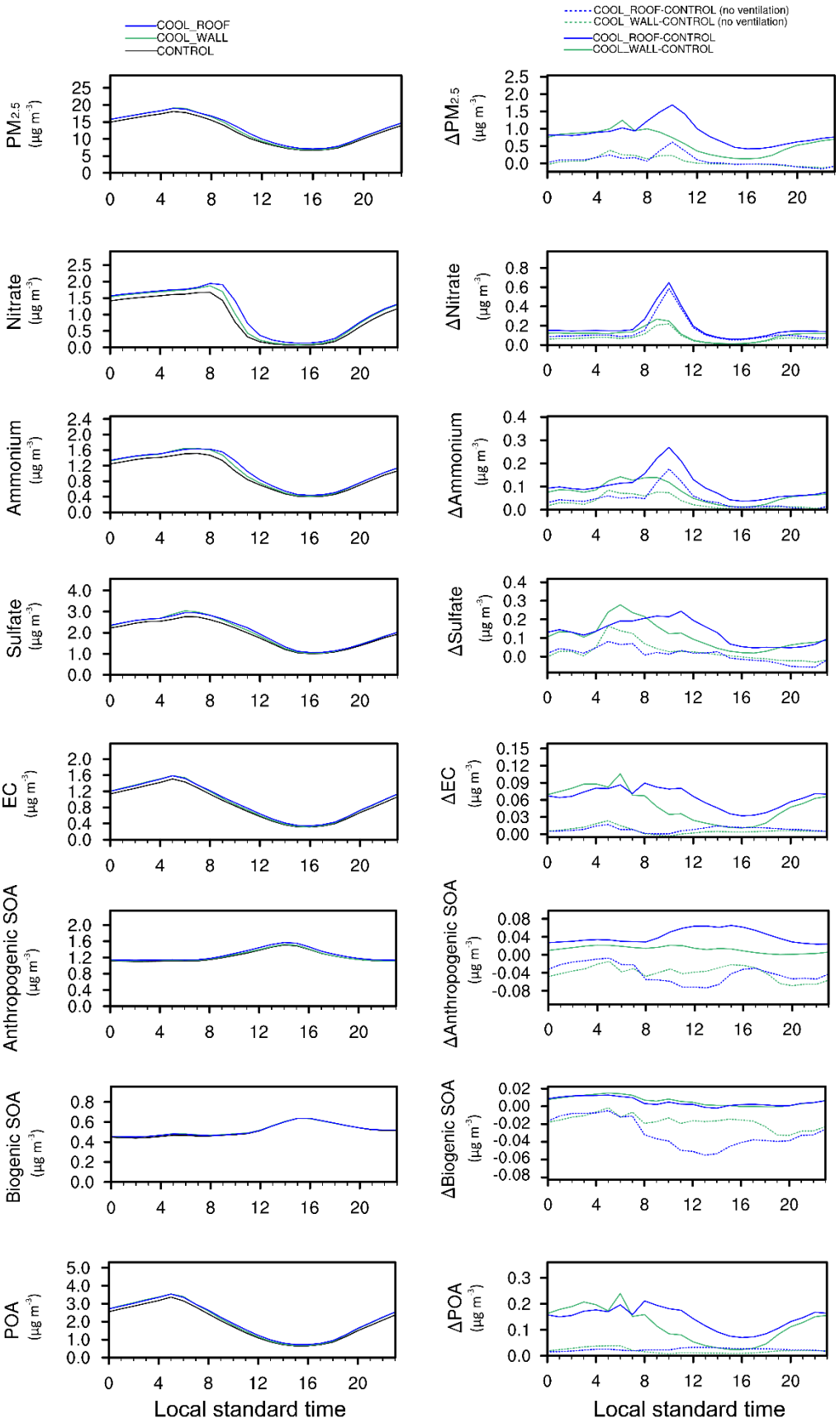
COOL_ROOF
COOL_WALL
CONTROL
COOL_ROOF-CONTROL (no ventilation)
COOL_WALL-CONTROL (no ventilation)
COOL_ROOF-CONTROL
COOL_WALL-CONTROL
PM2.5 (μg m-3)
ΔPM2.5 (μg m-3)
Nitrate (μg m-3)
ΔNitrate (μg m-3)
Ammonium (μg m-3)
ΔAmmonium (μg m-3)
Sulfate (μg m-3)
ΔSulfate (μg m-3)
EC (μg m-3)
ΔEC (μg m-3)
Anthropogenic SOA (μg m-3)
ΔAnthropogenic SOA (μg m-3)
Biogenic SOA (μg m-3)
ΔBiogenic SOA (μg m-3)
POA (μg m-3)
ΔPOA (μg m-3)
Local standard time
Local standard time

625

626 Figure 4. Diurnal cycles of spatially averaged $PM_{2.5}$ concentrations by species. The left column shows the
627 diurnal cycle of spatially averaged $PM_{2.5}$ ($\mu g\ m^{-3}$) for CONTROL, COOL_WALL, and COOL_ROOF. The right
628 column shows the differences in $PM_{2.5}$ species for COOL_WALL – CONTROL and COOL_ROOF – CONTROL
629 and the differences if ventilation effect is excluded. Values represent spatial averages in Los Angeles
630 County (i.e., shown in Figure S3b) for urban grid cells from 00:00 LST on July 3 to 00:00 LST on July 12.
631 Note that vertical axis ranges vary for each species.

632

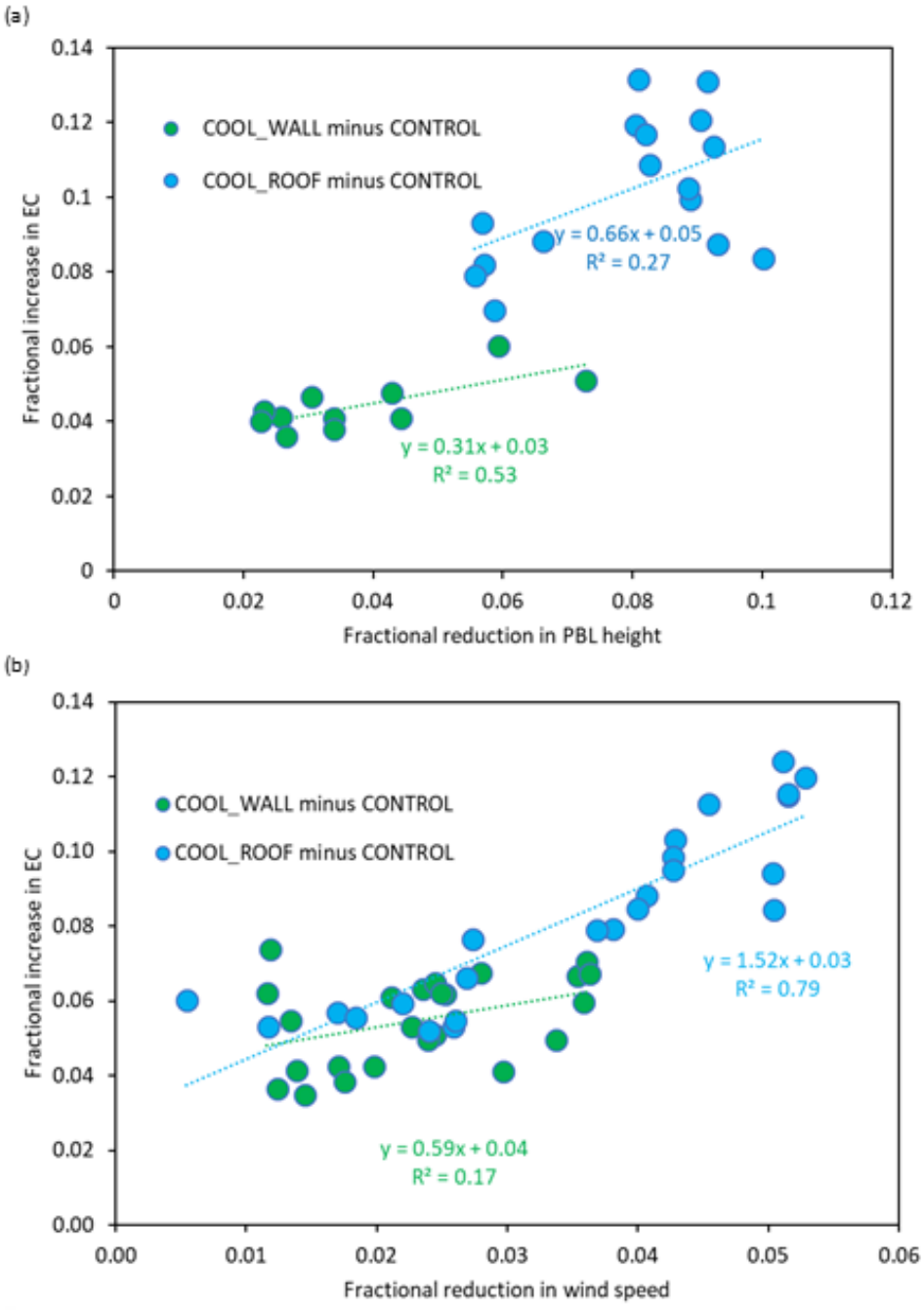

633

634 Figure 5. Scatter plots showing fractional increase in EC concentrations induced by cool walls and cool
635 roofs versus (a) fractional reduction in PBL height and (b) fractional reduction in 10-meter wind speed.
636 The value on each dot represents the hour of day (e.g., 9 = 09:00 LST). Least-squares linear regressions
637 and corresponding coefficients of determination (R^2) are also shown. Values represent spatial averages
638 in Los Angeles County (i.e., shown in Figure S3b) for urban grid cells from 00:00 LST on July 3 to 00:00
639 LST on July 12.